Dalton Transactions

Accepted Manuscript

ROYAL SOCIETY
OF CHEMISTRY

www.rsc.org/dalton

Photolytic Properties of Cobalamins:

A Theoretical Perspective

Pawel M. Kozlowski,[1,3,*] Brady D. Garabato,[1] Piotr Lodowski,[2] and Maria Jaworska[2]

[1]Department of Chemistry, University of Louisville, Louisville, Kentucky 40292,

United States

[2]Department of Theoretical Chemistry, Institute of Chemistry, University of Silesia,
Szkolna 9, PL-40 006 Katowice, Poland

[3] Visiting professor, Department of Food Sciences, Medical University of Gdansk, Al.
Gen. J. Hallera 107, 80-416 Gdansk, Poland

†Correspondence:
Prof. Dr. Pawel M. Kozlowski
University of Louisville
Department of Chemistry
2320 South Brook Street
Louisville, KY 40292, USA
pawel@louisville.edu

ABSTRACT

This Perspective Article highlights recent theoretical developments, and summarizes the current understanding of the photolytic properties of cobalamins from a computational point of view. The primary focus is on two alkyl cobalamins, methylcobalamin (MeCbl) and adenosylcobalamin (AdoCbl), as well as two non-alkyl cobalamins, cyanocobalamin (CNCbl) and hydroxocobalamin (HOCbl). Photolysis of alkyl-cobalamins involves low-lying singlet excited states where photodissociation of the Co-C bond leads to formation of singlet-born alkyl/cob(II)alamin radical pairs (RPs). Potential energy surfaces (PESs) associated with the low-lying excited states as a function of both axial bonds, provides the most reliable tool for initial analysis of the photochemical and photophysical properties of cobalamins. Due to the complexity, and size limitations associated with the cobalamins, the primary method for calculating ground state properties is density functional theory (DFT), while time-dependent DFT (TD-DFT) is used for electronically excited states. For alkyl cobalamins, energy pathways on the lowest singlet surface, connecting metal-to-ligand charge transfer (MLCT) and ligand field (LF) minima, can be associated with photo-homolysis of the Co-C bond observed experimentally. Additionally, energy pathways between minima and seams associated with crossing of S_1/S_0 surfaces, are the most efficient for internal conversion (IC) to the ground state. Depending on the specific cobalamin, such IC may involve simultaneous elongation of both axial bonds (CNCbl), or detachment of axial base followed by corrin ring distortion (MeCbl). The possibility of intersystem crossing, and the formation of triplet RPs is also discussed based on Landau-Zener theory.

1. Introduction

Biologically active forms of vitamin B_{12} (CNCbl, cyanobobalamin) such as methylcobalamin (MeCbl) or adenosylcobalamin [AdoCbl, (5'-deoxy-5'-adenosyl)cobalamin or coenzyme B_{12}] are highly complex organometallic molecules that contain a unique σ Co-C bond (Figure 1). The Co-C bond of alkyl cobalamins is of moderate strength, ranging from 30 to 44 kcal/mol, depending on the specific alkyl cobalamin, and experimental conditions for which bond dissociation energies (BDEs) have been determined.[1,2,3,4,5,6,7,8,9] MeCbl and AdoCbl are cofactors in a series of enzymes that catalyze complex molecular transformations, where the initial step involves cleavage of the organometallic Co-C bond.[10,11,12,13,14,15,16,17,18,19,20,21,22,23,24,25,26] In particular, MeCbl is the cofactor for a class of enzymes that catalyze the intermolecular methyl (Me) transfer reactions,[19,23,25] while AdoCbl-dependent enzymes catalyze rearrangement reactions mediated by radical intermediates.[17,18,20,21,26]

Cobalamins possess complex photochemical, and photophysical properties that are mediated by their electronically excited states.[27,28,29,30,31,32,33,34,35,36,37,38,39,40,41,42,43,44,45,46,47,48] The photo-homolysis of the Co-C bond in alkyl cob(III)alamins may be induced by wavelengths in the 300 – 530 nm range, absorbed by the corrin ring to generate cob(II)alamin and corresponding alkyl radicals. In particular, MeCbl or AdoCbl cofactors undergo photolysis upon excitation with visible or near UV light,[36,37,38,40] and in the case of MeCbl, the quantum yield of Co-C bond cleavage is wavelength dependent.[38,40] The specific mechanism of photolysis depends not only on the type of alkyl group, but also on the environment of the cofactor, such as solvent or enzyme.[39,41,43,44] In strongly acidic conditions the protonated lower dimethylbenzimidazole (DBI) axial base is replaced by water, leading to the formation of B_{12} cofactors in their base-off from. The photolytic properties of the base-off cobalamins are very different from those of their base-on analogues.[45] The absence of a DBI ligand alters the electronic structure of the cofactor and opens a channel for fast nonradiative decay, which effectively competes with Co-C bond photodissociation.

There are number of a light-triggered reactions mediated by alkyl cobalamins where photo-cleavage of the Co-C bond constitutes the initial step. Examples of such reactions involve photo-responsive reagents for drug delivery,[49,50,51,52] where a therapeutic agent attached to the

cobalt is released based on homolytic cleavage, or light-activated molecular switches.[53] A recently discovered and structurally characterized photoreceptor, CarH, uses the photolysis of AdoCbl as a light sensor to regulate the biosynthesis of carotenoids.[54,55] Photolysis of the Co-C bond leads to a large-scale conformational change of the CarH tetramer, that promotes direct binding with DNA. This change in conformation is unique for photoreceptors, and is more drastic than cis-trans isomerization or photo-induced electron transfer, requiring no additional proteins for regulation.

Of particular importance is the ability to probe the photolytic cleavage of the Co-C bond for enzyme-bound B_{12} cofactors, such as (AdoCbl)-dependent glutamate mutase (GLM)[56,57] and (AdoCbl)-dependent ethanolamine ammonia-lyase (EAL).[58,59,60,61] In (AdoCbl)-dependent enzymes homolytic cleavage of the Co-C bond is triggered by substrate binding, and coupled to subsequent hydrogen atom abstraction. In contrast, cleavage induced by light can generate similar radical pairs to those in enzymatic reactions, though without coupling to the subsequent abstraction step. Photolytic cleavage inside enzymatic environments thus creates cob(II)alamin and Ado radical pairs, as well as the ability to probe the mechanistic aspects of the corresponding B_{12}-dependent catalysis.[62]

In contrast to B_{12} cofactors, cobalamins with non-alkyl upper axial ligands, such as CN, are generally considered to be photostable.[42] Excitation of CNCbl results in the formation of a short-lived excited state that undergoes fast ground-state recovery on a picosecond time scale.[46] Interestingly, although hydroxocobalamin (HOCbl) is a non-alkyl cobalamin, it undergoes photolysis upon excitation with light above 300 nm.[63] HOCbl can be used as a potential source of hydroxyl radicals generated photochemically via homolytic cleavage of the Co-OH bond, where the photolytic mechanism involves competition between prompt dissociation, and internal conversion.[64] Such a strategy furnishes control over the initiation, and termination of radical production, simply by switching on/off the light source.

A detailed understanding of the photolytic processes of cobalamins requires both careful experimental study, and state-of-the-art quantum chemical calculations. Of primary importance is a detailed knowledge of the electronically excited states. In this Perspective, we will focus on recent computational studies,[65,66,67,68,69,70,71,72,73,74] and summarize the current understanding of photodissociation mechanisms from a theoretical point of view. The photolytic properties of

cobalamains primarily depend upon the nature of axial ligands, with photodissociation of their upper ligands mediated by their corresponding low-lying excited states. Four systems, two alkyl cobalamins, MeCbl and AdoCbl, as well as two non-alkyl cobalamins, CNCbl and HOCbl, will receive special attention.

2. Structural Models

Despite advances in computational methods, cobalamins are still considered complex for theoretical studies, especially in regards to their low-lying excited states. Such complexity is due to the presence of the partially conjugated corrin macrocycle, which involves extensive mixing between the π orbitals of corrin and the d orbitals of cobalt. Depending on the nature of their upper axial ligands (Figure 1), B_{12} cofactors may range in size from 183 atoms (MeCbl) to 209 atoms (AdoCbl). The tractability of these calculations typically requires the use of truncated models, specifically with respect to side chains and the nucleotide loop. Initial structures are typically derived from high-resolution X-ray crystallographic data[75,76,77,78,79] by replacing all side chains of the corrin ring with hydrogen atoms.[80,81] Since the nucleotide side chain containing the negatively charged PO_4^- is omitted, the resulting structural model, denoted B-[Co^{III}corrin]-R$^+$, has a total charge of +1 (Figure 1). The lower DBI axial base is also typically replaced by imidazole (Im), or water in the case of the base-off forms.

Truncation is also important in wavefunction-based approaches, such as complete active space self-consistent field (CASSCF), where the cost of computations strongly depends on the size of the active space. It has been shown that multi-configurational methods may be applied to accurately predict low-lying excited state properties.[82,83,84] This strategy is particularly valuable for benchmarks including different upper axial ligands in the multi-configurational active space. In some instances, such as the analysis of spin-orbit coupling (SOC) effects, where coupling between singlet and triplet electronic excited states may occur, corrin structural models are further truncated to the inner-conjugated macrocycle.[74]

3. Computational Methods

Due to the size and the complexity of the cobalamins (Figure 1), DFT is currently the most widely used computational tool to study their ground-state properties, while TD-DFT is employed to study the corresponding low-lying excited states.[85,86,87,88,89] However, a question that commonly arises with TD-DFT applied to such complex systems containing transition metals, is how appropriate are the excited state descriptions.

It is important to recall that one of the key features of the B_{12} cofactors is the bond dissociation energy (BDE) of the Co-C bond, which has received considerable attention both experimentally and computationally. It has been shown that theoretical Co-C BDEs are very sensitive to the applied exchange-correlation functional.[90,91] Hybrid DFT functionals with a substantial amount of the Hartree-Fock (HF) exchange, such as the popular B3LYP, considerably underestimate Co-C BDEs with a magnitude of error proportional to the HF exchange in the functional. One the other hand, the use of the GGA-type functionals leads to significant improvements over B3LYP-based calculations. Dispersion corrections are also important for the accurate predictions of Co-C BDEs. Of all DFT functionals examined, the most accurate descriptions of Co-C bond breaking in the MeCbl cofactor were provided by the B97-D, and BP86 with D3 correction, functionals.[92,93,94,95]

Electronically excited states have also been the subject of several benchmark calculations, including the CNCbl and MeCbl systems.[82,83] Reported benchmark analysis targets either a specific electronically excited state, such as for MeCbl,[83] or a low-lying manifold of electronically excited states, such as for CNCbl.[82] Initial analysis of the S_1 state for MeCbl using B3LYP suggested a pure $\pi \rightarrow \pi^*$ character,[96] while BP86 benchmarked with *ab initio* calculations predicts a metal-to-ligand charge-transfer (MLCT) state as a result of mixing Co d orbitals with corrin π. This predicted MLCT nature of the S_1 state in MeCbl is consistent with the interpretation based on transient absorption spectroscopy.[36,38,40,42] Different functionals were used to reproduce the CNCbl spectrum up to 250 nm, and four states were specifically targeted for comparison with wavefunction based calculations, where it was concluded that BP86 also provides the most appropriate description of the electronic properties of CNCbl.[82]

Multi-configurational methods also offer a way to extend the range of cobalamin excited state PESs to dissociated axial bond distances past the TD-DFT limit, which is of particular interest for the base-off cobalamins. Although size limitations of the active space prevent the use of full structures, truncated models have generally been shown to correlate well with TD-DFT descriptions at the implicit solvent level, including interactions with individual solvent molecules. The explicit treatment of environment in cobalamin excited state calculations is also of interest, particularly for states at dissociated axial bond distances, and for cofactors such as AdoCbl where the S_1 state is sensitive to environmental conditions, with corresponding excited states that may differ from those in solution. Theoretical descriptions of both the ground and excited states of cobalamins inside biological environments, in many cases remains a challenge, due to the scalability of system size, and the sensitivity of available methods to input parameters. Further studies using methods such as QM/MM are expected to provide insight into the energetics of these complex cobalamin systems.

4. Axial Bond Lengths of Cobalamins Corresponding to S_0 and S_1 and States

Cobalamins have been the subject of several structural investigations using DFT, and the availability of extensive structural data has been used to theoretically determine the effects axial bonding within the corrin system. The nature of the upper axial ligand determines the corresponding axial bond lengths, which are in fact the most sensitive parameters with respect to overall structural change. It has been shown that the BP86 functional reproduces experimental axial bond lengths very well, and based on this data, ground state properties of the cobalamins have been further rationalized by correlating axial bond distances in terms of *inverse vs. normal trans influence*.[97] On the other hand the corrin structure is relatively insensitive to the nature of the upper axial ligand, and the bulkiness of the upper ligand changes only the planarity of the corrin ring.

Figure 2 shows a comparison of experimental,[75,76,77,78] and DFT/BP86-based Co-R, and Co-N$_{Im}$ bond lengths for ground states of the four cobalamins under consideration. As seen, for the S_0 state, reproduction of Co-R bond lengths is more accurate than for Co-N$_{axial}$ distances. The prediction of Co-N$_{axial}$ distances are reasonable however, as their lengths are more sensitive with

respect to structural simplifications, and local environments. Although predicted Co-N_{axial} bond lengths are generally more sensitive to the local environment,[98] BP86 is considered to reproduce them very well.

Because there is no structural data available for the excited states of cobalamins, we need to rely on calculations to predict their structures. Figure 2 also shows the TD-DFT/BP86 optimized axial bond lengths corresponding to the S_1 state. Predicted changes for alkyl cobalamins indicate that Co-N_{Im} distances of the optimized S_1 states are shorter, while Co-C bond lengths for both MeCbl and AdoCbl are longer in comparison to the ground state. Changes in axial bonding in the S_1 state for non-alkyl cobalamins are less systematic. Significant lengthening of Co-CN and Co-N_{Im} bonds is observed in the case of CNCbl. Opposite changes are predicted for HOCbl, where both Co-OH and Co-N_{Im} are slightly shorter for S_1 in comparison to S_0. The extent of lengthening for CNCbl however is much larger in comparison to the shortening predicted for HOCbl.

5. Potential Energy Surfaces with Respect to Axial Bonds Lengths

Taking into account that upon electronic excitation the largest structural changes occur in axial bonding, potential energy surfaces (PESs) constructed as functions of both axial bonds, provide the most reliable tool for initial analysis of the photophysical properties of the cobalamins. [66,67,68,69,70,71,72] Figure 3 shows PESs for the S_0, S_1, and S_2 states of each of the four cobalamins under consideration. To obtain these surfaces, the structure of B-[Co^{III}corrin]-R^+ that corresponds to the energy minimum (S_0) is used as a starting point, and the axial bonds are systematically elongated and fixed with all other coordinates optimized, typically in the presence of an implicit solvent. Low-lying excites states are then generated as vertical excitations, and orbital analysis for these points are used to characterize surface regions were excitations are close in energy. Using TD-DFT it is possible to optimize the lowest excited state corresponding to S_1, although attempts to optimize the S_2 and higher states have been unsuccessful due to technical issues. Previous calculations have shown that optimized S_1 PESs are similar to their corresponding surfaces generated as vertical excitations.[83] Therefore, vertical excitations are typically used to describe S_1, as well as S_2, and higher electronically excited state surfaces.

Based on the PESs shown in Figure 3, some general trends may be noted. The energy gap between the S_1 and S_0 surfaces is considerably larger for the alkyl cobalamins than for non-alkyl cobalamins. Increased proximity of S_1 to S_0 for ligand field states results in an energy path suitable for rapid internal conversion (IC) to the ground state, as in the case of CNCbl.

The S_1 PESs of the alkyl coblamins may also be noted as having a seam separating two minima regions. This seam arises from a crossing of S_1 surfaces corresponding to MLCT character near the minimum, and ligand field (LF) character at elongated axial bond distances. In the case of MeCbl, the LF region is energetically shallow, and also slightly higher in energy than the minimum. For AdoCbl it may be seen that the S_1 LF minimum is energetically similar to the S_1 MLCT minimum, which is shallow with respect to upper ligand, indicating a possible preference for the base-off form in the LF excited state. Photodissociation occurs from the LF states because they involve d-d excitations resulting in increased antibonding character with respect to the Co-R ligand. Thus, the energy minimum pathways connecting minima corresponding to MLCT, and LF regions of the S_1 PESs are most relevant. The S_2 PESs of the alkyl cobalamins MeCbl and AdoCbl may be seen as similar, each with one shallow minima, indicating preferences towards elongated $Co-N_{Im}$ bond lengths. The S_2 PESs, and higher excited state surfaces are thus also important to explain the wavelength dependence of photodissociation in each system.

The S_1 PESs of the non-alkyl cobalamins on the other hand, have shallow minima with respect to $Co-N_{Im}$ coordinate. In the case of CNCbl both minima are LMCT, and the S_1 PES is very sensitive with respect to solvent, with one shallow minimum that with respect to elongated axial base. The S_1 PES of HOCbl on the other hand, has two minima, one corresponding to MLCT/ LL at short axial bond distances that resembles MeCbl, and the other corresponding to LMCT/LF at elongated $Co-N_{Im}$ distances. Another possible minima may be noted in HOCbl, which is shallow with respect to elongated Co-OH distances, and may result in a possible photodissociation pathway, though this region cannot effectively be explored due to the limitations associated with the TD-DFT methodology.

Excited state PESs at the TD-DFT level may be used to validate the experimentally determined photodynamics of the alkyl and non-alkyl cobalamins. Our current understanding of

the PESs of the cobalamins under consideration will be summarized in further detail below, highlighting experimental data, and emphasizing current directions in theory.

6. Methylcobalamin

Femtosecond to nanosecond transient absorption spectroscopy have been applied to investigate the primary photochemistry of the base-on MeCbl cofactor, and its photolysis at excitation wavelengths near the UV (~ 400 nm) and visible regions (~ 520 nm).[36,38,40] Excitation at 400 nm leads to partitioning between prompt Co-C bond photolysis (~ 25%), and the formation of a metastable cob(III)alamin photoproduct, a low-lying electronic state with a nanosecond lifetime. Excitation at 520 nm results only in formation of the metastable cob(III)alamin photoproduct, with no prompt bond homolysis observed. Experimentally the low-lying S_1 state in MeCbl is best characterized as a $d/\pi \rightarrow \pi^*$ MLCT-type excitation. In strongly acidic conditions (pH ~ 2), where MeCbl adopts the base-off form, photochemical properties of MeCbl are very different from those of the base-on analogues.[45] The absence of the DBI axial base alters the electronic properties of MeCbl, and as a consequence, a channel for fast nonradiative decay is opened, which effectively competes with the channel for Co-C bond photodissociation.

The photolytic properties of MeCbl may be readily explained in terms of the PESs associated with low-lying excited states.[71,72] Figure 4 shows a two-dimensional projection of the S_1 surface extended to longer axial bond distances, to regions that cannot be explicitly explored by TD-DFT calculations due to the inadequacy in describing weak elongated covalent bonds. In addition to the S_1 surface of base-on MeCbl, the S_1 surface corresponding to the base-off form is also shown, where one of the axial coordinates is the Co-OH$_2$ distance. Regardless of specific base-on/off form, TD-DFT calculations identify two regions relevant to the observed photochemistry of MeCbl. The first region corresponds to shorter axial bond lengths, MLCT-type transitions characterized as $(d_{xz}/d_z^2 + \pi) \rightarrow \pi^*$ excitations, while the second region corresponds to longer bond distances, characterized as LF-type $(d_{yz} + \pi) \rightarrow \sigma^*(d_z^2)$ excitations

involving mainly d → d transitions of cobalt. The LF portions of the S_1 PES, an electronic state of MeCbl primarily responsible for photolytic cleavage of the Co-C bond, is characterized by substantial elongation, or even detachment of axial base. The energetic preferences for base-on/off are quite different however, as can be deduced from the PESs associated with both S_1 states. The energy minimum associated with the S_1 PES of MeCbl in the base-on form is an MLCT state, while the base-off form has a much stronger preference for the LF state (Figure 4). Since the LF state is antibonding with respect to ligands it can be concluded that photodissociation should occur much easier from MeCbl in its base-off form. On the other hand, this state is also prone to IC for the same reason, and hence the large tendency for deactivation.

The base-on form of MeCbl has two possible photodissociation pathways which can be identified on the basis of energetic grounds. These pathways are distinguished by whether the Co-C bond (path A), or Co-N_{Im} bond (path B) elongates first. The wavelength dependence of MeCbl photolysis can be associated with these specific pathways. Excitation using visible light (520 nm) can be associated with Path A, whereas excitation in the near-UV region (400 nm) with Path B. In contrast, only Path B is active in the base-off form of MeCbl. Path A is inactive due to the energy barrier associated with direct dissociation of the methyl ligand, which is higher than the barrier of intersection between the MLCT and LF electronic states.

There are several intermediates along Path B, which have been located and characterized by TD-DFT calculations. Of particular importance and relevance to MeCbl photochemistry is the point labeled IIIB (S_{1min}), which appears as a common feature regardless of the base-on/off configuration. This point corresponds to the S_1 energy minimum with detached axial base. The optimized geometry of this intermediate in the S_1 state has a significantly elongated Co-C bond in comparison to the ground-state, 2.23 Å vs. 1.97 Å, respectively. According to TD-DFT calculations, from this intermediate, either homolytic cleavage of the Co-C bond may take place, or IC to the ground state. To explore the mechanism of IC, internal coordinates associated with corrin ring distortion, in addition to Co-C distance, are required to describe changes associated with the coordination sphere of cobalt. The bending N_{12}-Co-N_{23} angle can be selected as the geometrical parameter associated with the domed distortion of the corrin macrocycle in the excited state. The energy map constructed as a function of Co-C distance, and N_{12}-Co-N_{23} bend

angle, reveals that the PESs associated with the S_0 and S_1 states possess an intersection seam, and thus an effective energetic pathway associated with S_1/S_0 conversion can be located.

7. Adenosylcobalamin

The size and the complexity of the Ado ligand (Figure 1), makes characterization of AdoCbl excited states a more challenging task in comparison to other cobalamins.[99,100] One of the primary difficulties in determining the low-lying excited states of AdoCbl, is related to the presence of long-range CT states between the corrin, and Ado moieties which are significantly underestimated by TD-DFT calculations due to errors associated with self-interaction. Preliminary investigations performed for a structural model of AdoCbl, where the Ado upper ligand was simplified to ribose (Rib),[69] revealed that the S_1 and S_2 states of RibCbl should not be significantly different from those predicted for MeCbl. The S_1 state was found to have dominant MLCT character, consistent with experimental findings.

However, this is not the case as analysis of experimental data for AdoCbl and MeCbl points out a number of differences related to their photochemistry.[37,39,40] The photolysis of AdoCbl is wavelength independent in contrast to MeCbl, and the S_1 state is also sensitive to environmental conditions.[43] Specifically, according to transient absorption spectroscopy, the S_1 state of AdoCbl in ethylene glycol resembles a spectrum with elongated axial bonds. This state is also observed in water, with implications that the axial base is detached. On the other hand, in the enzymatic environment, the S_1 state resembles that of MeCbl.[47]

The S_1 surface computed for AdoCbl as shown in Figure 3 may give insight into the aforementioned properties of the S_1 state observed experimentally. The two minima observed on the S_1 surface of AdoCbl may be associated with different environmental conditions. The region with elongated axial bonds on the S_1 PES seems to be consistent with experimental observations in water, due to the observed stabilization of this LF state. The MLCT minimum on the S_1 surface however is more consistent with (AdoCbl)-dependent GLM. More computational studies both for isolated AdoCbl, and AdoCbl inside enzymatic environments using QM/MM approaches, are expected to provide better insight. Further study is required computationally to explain why AdoCbl photolysis is wavelength independent. Although this remains an open issue,

preliminary investigations indicate that this may be related to a higher density of excited states within the same energy region for AdoCbl, in comparison to MeCbl.

8. Cyanocobalamin

The electronic excited states, and IC of CNCbl have been thoroughly investigated using ultrafast spectroscopy.[42,46] CNCbl is one of most well characterized cobalamins by high-quality transient IR, and UV-Vis, in the range of 266 to 590 nm. Most notably the CNCbl system is photostable, and the Co-CN bond does not photo-dissociate under simple photon excitation. Instead, electronic excitation results in IC through a cascade of states involving the π/d orbitals of corrin and Co to the ground state, through a short-lived LMCT intermediate. This S_1 state has decay rates which are both temperature and solvent dependent, with increasing lifetimes in less polar solvents. In water at room temperature, the experimentally determined barrier to IC is 2.1 kcal/mol, and occurs on a 6.7 ± 0.2 ps time scale. The LMCT intermediate of CNCbl is a key photochemical state observed experimentally, and is characterized as $\pi \rightarrow \sigma^*$ (d_z^2) LMCT.

The PESs calculated by TD-DFT (Figure 4) are considered to describe the excited state dynamics of CNCbl very well in accord with experimental results.[67,70] The optimum energy path, which effectively results in IC to the ground state, essentially lies on a diagonal cut bisecting the 3D PES, as shown in Figure 5. Analysis of the excited state manifold of CNCbl reveals that initial excitation results in Franck-Condon population of higher $\pi \rightarrow \pi^*$ states, followed by decay to an intermediate $\pi \rightarrow d$ LMCT state. Decay to this $\pi \rightarrow d$ LMCT intermediate results in only a slight elongation of both axial bond lengths, corresponding to 1.857 to 1.900 Å for Co-C, and 2.054 to 2.096 Å for Co-N$_{Im}$ changes labeled A and B in Figure 5, respectively. This $\pi \rightarrow d$ LMCT state then relaxes along the S_1 surface to a very shallow $\pi \rightarrow \sigma^*$ (d_z^2) LMCT minimum with a more pronounced structural change, corresponding to elongated bond lengths of 2.216 for Co-C, and 2.275 for Co-N$_{Im}$, structure C, Figure 5. Further axial bond elongation from this LMCT minimum does not lead to photodissociation, but rather a crossing of the S_0 state with S_1 at a Co-C distance of 2.650 Å, and Co-N distance of 2.55 Å, that effectively leads to IC. The energy barrier between the S_1 minimum and the S_1/S_0 crossing point, was estimated to be around

5 kcal/mol, which can be compared directly with the experimental value of 2.1 ± 0.2 kcal/mol in water at room temperature, based on a dielectric constant of 80.

9. Hydroxocobalamin

HOCbl has received special attention after it was demonstrated that it may be converted with light to cob(II)alamin, and hydroxyl radicals.[63] As a result, HOCbl can function as photocatalytic source of hydroxyl radicals for the investigation of DNA and RNA. In particular, photochemically generated radicals may be used for the cleavage of supercoiled DNA to its relaxed form. Electronically excited states of HOCbl have also been thoroughly investigated using ultrafast excited state dynamics.[47] As a non-alkyl cobalamin, HOCbl was found to be generally photostable, with radicals generated for shorter wavelengths, namely < 350 nm. The mechanism of hydroxyl radical formation involves competition between prompt Co-OH bond photodissociation, and IC.

To explore the nature of the low-lying excited states of HOCbl, TD-DFT calculations were applied to obtain corresponding PESs as a function of both axial bonds. Figure 3d shows 3D energy map contours, while Figure 6 shows the projection of the S_1 state along with possible energy paths. Overall the low-lying excited states of HOCbl are similar to those associated with CNCbl. For example, the proximity of the S_0 and S_1 states at longer axial bond distances are similar for both systems, with a shallowness of energy minima towards longer $Co-N_{Im}$ distances on the S_1 surfaces. However, some other features are more in line with alkyl cobalamins, such as two energy minima located on S_1. The energy surface corresponding to the lowest S_1 excited state consists of at least three different electronic states. Two of them can be associated with energy minima, one at shorter Co-OH and $Co-N_{Im}$ axial bond lengths (B), and the second with slightly elongated Co-OH and much longer $Co-N_{Im}$ distances (C). The third minimum corresponds to Co-OH distances longer than 2.7 Å, and within a $Co-N_{Im}$ range of 1.9 − 2.2 Å. This part of the S_1 surface has a dissociative character. Orbital analysis of the corresponding electronic excitations reveals that the minimum energy of the S_1 state has dominant $p_{OH}/d \rightarrow \pi^*$ character at short Co-OH distances. Upon Co-OH bond elongation, the S_1 state crosses with

higher excited states that have dominant σ* contributions. This changes the character from $p_{OH}/d \rightarrow \pi^*$ to $p_{OH}/d \rightarrow \sigma^*$. For long Co-OH distances, the S_1 surface has mainly $p_{OH} \rightarrow \sigma^*$ character, with a small contribution from the d orbital of cobalt.[68]

The proximity of S_1/S_0 surfaces may lead to deactivation through two possible channels (Figure 6). The first involves simultaneous elongation of both axial bonds, the path denoted $B(S_{1min}) \rightarrow C(S_1) \rightarrow D(S_1)$, a mechanism similar to that observed in CNCbl. The second involves elongation and detachment of the axial base followed by corrin ring distortion, the path denoted $B(S_{1min}) \rightarrow C(S_1) \rightarrow E(S_{1min})$, a mechanism similar to MeCbl. On the other hand, a dissociative pathway cannot be reached from $B(S_{1min})$ for energetic reasons, and must involve higher electronically excited states. Thus, it can be inferred that excitations using longer wavelengths leads effectively to population of the energy minimum corresponding to $p_{OH}/d \rightarrow \pi^*$, which is primarily responsible for deactivation. Excitations with shorter wavelengths can populate a repulsive electronic state, with likely dominant $p_{OH}/d \rightarrow \sigma^*$ or $d/p_{OH} \rightarrow \sigma^*$ character, that at longer Co-OH distances becomes dissociative.

10. Involvement of triplet states

Up to this point the photolytic properties of alkyl cobalamins have been presented in terms of their low-lying singlet excited states, resulting in generation of singlet-born alkyl/cob(II)alamin radicals, as consistent with experimental studies.[44] Specifically, the magnetic field effect implies that upon excitation, a singlet radical pair is formed, and photodissociation should not change the overall spin character of the radical pairs.[101] A prominent geminate recombination also implies that the radical pairs generated are singlets. However, involvement of triplet states cannot be precluded on theoretical grounds, particularly for the base-off forms of the B_{12} cofactors.

To assess the feasibility of the involvement of triplet states, semi-qualitative descriptions are presented based on Landau-Zener (LZ) theory.[102] According to LZ theory, the crossing probability between two adiabatic PESs i and j is given by:

$$P_{ij} = \frac{-2\pi \left| H_{ij} \right|^2}{\hbar F_{ij} \left| \frac{dR}{dt} \right|}, (1)$$

where H_{ij} is the spin-orbit coupling matrix element, (dR/dT) is the product of the crossing speed, and (F_{ij}) is the difference in slope between states involved in the crossing defined as:

$$F_{ij} = \left| \frac{dE_i}{dR} - \frac{dE_j}{dR} \right| . (2)$$

The probability of spin-forbidden crossover involving transition metals depends on the nature of PESs near the minimum-energy crossing point (MECP). Specifically the P_{ij} increases when the gradient (or slope) between diabatic surfaces is small with respect to the MECP, and decreases when the gradient is large. Closer inspection of energy curves computed as a function of Co-C bond distances for base-on/off forms reveals that this condition regarding the MECP is best fulfilled for the base-off form, as exemplified for MeCbl, where the optimized S_1 state is very shallow, and in close proximity to a number of triplet states (Figure 7).

According to El-Sayed rules, orbitals involved in spin-crossover should be of the same type, but rotated by 90°.[103,104] Two excited state regions near the MECP corresponding to R(Co-C) = 1.90 Å, and R(Co-C) = 2.15 Å, are shown for base-off MeCbl in Figure 7. S_1, and T_3 states fulfill these conditions, and may mix to form SOC states before, and after the MECP. At further distances, S_1 may also mix with a repulsive $^3\sigma\rightarrow\sigma^*$ state. The repulsive $^3\sigma\rightarrow\sigma^*$ state at the TD-DFT level drops in energy towards the ground state due to the instability associated with the wavefunction. However, caution should be taken regarding this state, which at the multi-configurational level has proper asymptotic behavior towards the dissociation limit.

To determine the extent of SOC near the MECP, and at dissociated Co-C distances for base-off cobalamins, the use of multireference methods have been employed. SOC states composed of singlet-triplet pairs, or triplet-triplet pairs may then mix due to the relativistic nature of the Hamiltonian. According to preliminary calculations,[74] SOC with significant magnitudes (around 300 cm^{-1}) indicate that ISC is possible near MECPs at both short, and

elongated Co-C distances, where two pathway types, singlet $\rightarrow$ triplet $\rightarrow {}^3(\sigma \rightarrow \sigma^*)$, and singlet $\rightarrow {}^3(\sigma \rightarrow \sigma^*)$ may lead to photodissociation.

11. Summary and outlook

The photo-homolysis of the Co-C bond in alkyl cobalamins, such as MeCbl or AdoCbl, was first noted fifty years ago.[105,106,107,108] Since then, the ability to generate radicals via light has become the subject of vast experimental research. It is now generally accepted that the photolysis of alkyl cobalamins results in formation of cob(II)alamin and alkyl radical pairs, similar to the intermediates from (AdoCbl)-dependent enzymatic catalysis. On the other hand non-alkyl cobalamins are generally photostable, with HOCbl being the exception, when using short wavelength excitations, which generate hydroxyl radicals.

The photolysis of cobalamins depends upon a number of factors, such as the nature of both axial ligands, the local environment, and the excitation wavelengths applied. The mechanisms of photolysis at the molecular level represent a complex problem, and only recently has it become possible to use computational methods to understand the photolytic properties of cobalamins, and provide a detailed comparison with experiment. Preliminary results for the four cobalamins in this Perspective are very promising, and provide a more in-depth understanding of recent experimental results.

However, there are a number of open issues that remain to be addressed. The most important from a theoretical perspective, are related to AdoCbl, which still requires better connection with experiment. Current investigations are underway to extend the understanding of other cobalamins such as ethyl, aqua and azido, due to the availability of high quality experimental data. Although it is argued that the first and most important mechanistic description requires PESs as functions of axial bond lengths, consideration of different internal coordinates may also be needed. This is particularly important for the base-off forms of cobalamins, when considering mechanisms of internal conversion. Furthermore, although the majority of the discussion presented was of singlet states, involvement of triplets cannot be precluded, where better understanding is required from experimental studies. Another important area is the elucidation of photodynamic mechanisms inside biological environments, such as the

GLM, EAL, and CarH proteins, where QM/MM approaches are expected to provide valuable insights into these complex photosystems.

Acknowledgements

References

1. R. G. Finke and B. P. Hay, *Inorganic Chemistry*, 1984, **23**, 3041-3043.
2. C. D. Garr and R. G. Finke, *Inorganic Chemistry*, 1993, **32**, 4414-4421.
3. B. P. Hay and R. G. Finke, *Journal of the American Chemical Society*, 1986, **108**, 4820-4829.
4. B. D. Martin and R. G. Finke, *Journal of the American Chemical Society*, 1992, **114**, 585-592.
5. R. R. Hung and J. J. Grabowski, *Journal of the American Chemical Society*, 1999, **121**, 1359-1364.
6. B. P. Hay and R. G. Finke, *Journal of the American Chemical Society*, 1987, **109**, 8012-8018.
7. C. D. Garr and R. G. Finke, *Journal of the American Chemical Society*, 1992, **114**, 10440-10445.
8. I. J. Kobylianskii, F. J. Widner, B. Kraeutler and P. Chen, *Journal of the American Chemical Society*, 2013, **135**, 13648-13651.
9. S. Chowdhury and R. Banerjee, *Biochemistry*, 2000, **39**, 7998-8006.
10. D. Dolphin, *B12*, John Wiley & Sons, New York 1982.
11. J. Halpern, *Science*, 1985, **227**, 869-875.
12. R. Banerjee, *Chemistry & Biology*, 1997, **4**, 175-186.
13. M. L. Ludwig and R. G. Matthews, *Annual review of biochemistry*, 1997, **66**, 269-313.
14. B. Krautler, D. Arigoni and B. T. E. Golding, *Vitamin B_{12} and B_{12} Proteins*, Wiley-VCH, New York, 1998.
15. L. G. Marzilli, in *Bioinorganic Catalysis*, ed. J. B. Reedijk, E., Marcel Dekker Inc, New York, 1999, pp. 423-468.
16. R. Banerjee, *Chemistry and Biochemistry of B12*, John Wiley & Sons, New York, 1999.
17. T. Toraya, *CMLS, Cell. Mol. Life Sci.*, 2000, **57**, 106-127.
18. R. Banerjee, *Biochemistry*, 2001, **40**, 6191-6198.
19. R. G. Matthews, *Accounts of Chemical Research*, 2001, **34**, 681-689.
20. R. Banerjee, *Chemical Reviews*, 2003, **103**, 2083-2094.
21. T. Toraya, *Chemical Reviews*, 2003, **103**, 2095-2128.
22. K. L. Brown, *Chemical Reviews*, 2005, **105**, 2075-2150.
23. R. G. Matthews, M. Koutmos and S. Datta, *Current Opinion in Structural Biology*, 2008, **18**, 658-666.
24. L. Randaccio, S. Geremia, N. Demitri and J. Wuerges, *Molecules*, 2010, **15**, 3228-3259.
25. R. G. Matthews, *Metal Ions in Life Sciences*, 2009, **6**, 53-114.
26. E. N. G. Marsh and G. D. R. Melendez, *Biochimica Et Biophysica Acta-Proteins and Proteomics*, 2012, **1824**, 1154-1164.
27. J. F. Endicott and T. L. Netzel, *Journal of the American Chemical Society*, 1979, **101**, 4000-4002.
28. Y. Sakaguchi, H. Hayashi and Y. J. I'Haya, *The Journal of Physical Chemistry*, 1990, **94**, 291-293.
29. E. F. Chen and M. R. Chance, *Journal of Biological Chemistry*, 1990, **265**, 12987-12994.

Dalton Transactions Accepted Manuscript

30. E. Chen and M. R. Chance, *Biochemistry*, 1993, **32**, 1480-1487.

31. 1-2, 1993.

32. A. M. Chagovetz and C. B. Grissom, *Journal of the American Chemical Society*, 1993, **115**, 12152-12157.

33. G. R. Kinsel, L. M. Preston and D. H. Russell, *Biological Mass Spectrometry*, 1994, **23**, 205-211.

34. W. B. Lott, A. M. Chagovetz and C. B. Grissom, *Journal of the American Chemical Society*, 1995, **117**, 12194-12201.

35. E. Natarajan and C. B. Grissom, *Photochemistry and Photobiology*, 1996, **64**, 286-295.

36. L. A. Walker, J. T. Jarrett, N. A. Anderson, S. H. Pullen, R. G. Matthews and R. J. Sension, *Journal of the American Chemical Society*, 1998, **120**, 3597-3603.

37. L. A. Walker, J. J. Shiang, N. A. Anderson, S. H. Pullen and R. J. Sension, *Journal of the American Chemical Society*, 1998, **120**, 7286-7292.

38. J. J. Shiang, L. A. Walker, N. A. Anderson, A. G. Cole and R. J. Sension, *Journal of Physical Chemistry B*, 1999, **103**, 10532-10539.

39. L. M. Yoder, A. G. Cole, L. A. Walker and R. J. Sension, *The Journal of Physical Chemistry B*, 2001, **105**, 12180-12188.

40. A. G. Cole, L. M. Yoder, J. J. Shiang, N. A. Anderson, L. A. Walker, M. M. Banaszak Holl and R. J. Sension, *Journal of the American Chemical Society*, 2002, **124**, 434-441.

41. R. J. Sension, D. A. Harris and A. G. Cole, *The Journal of Physical Chemistry B*, 2005, **109**, 21954-21962.

42. J. J. Shiang, A. G. Cole, R. J. Sension, K. Hang, Y. Weng, J. S. Trommel, L. G. Marzilli and T. Lian, *Journal of the American Chemical Society*, 2006, **128**, 801-808.

43. D. A. Harris, A. B. Stickrath, E. C. Carroll and R. J. Sension, *Journal of the American Chemical Society*, 2007, **129**, 7578-7585.

44. A. B. Stickrath, E. C. Carroll, X. Dai, D. A. Harris, A. Rury, B. Smith, K.-C. Tang, J. Wert and R. J. Sension, *The Journal of Physical Chemistry A*, 2009, **113**, 8513-8522.

45. J. Peng, K.-C. Tang, K. McLoughlin, Y. Yang, D. Forgach and R. J. Sension, *The Journal of Physical Chemistry B*, 2010, **114**, 12398-12405.

46. T. E. Wiley, B. C. Arruda, N. A. Miller, M. Lenard and R. J. Sension, *Chinese Chemical Letters*, 2015, **26**, 439-443.

47. A. S. Rury, T. E. Wiley and R. J. Sension, *Accounts of Chemical Research*, 2015, **48**, 860-867.

48. A. R. Jones, H. J. Russell, G. M. Greetham, M. Towrie, S. Hay and N. S. Scrutton, *The Journal of Physical Chemistry A*, 2012, **116**, 5586-5594.

49. W. J. Smith, N. P. Oien, R. M. Hughes, C. M. Marvin, Z. L. Rodgers, J. Lee and D. S. Lawrence, *Angewandte Chemie-International Edition*, 2014, **53**, 10945-10948.

50. T. A. Shell, J. R. Shell, Z. L. Rodgers and D. S. Lawrence, *Angewandte Chemie-International Edition*, 2014, **53**, 875-878.

51. Z. L. Rodgers, R. M. Hughes, L. M. Doherty, J. R. Shell, B. P. Molesky, A. M. Brugh, M. D. E. Forbes, A. M. Moran and D. S. Lawrence, *Journal of the American Chemical Society*, 2015, **137**, 3372-3378.

52. T. A. Shell and D. S. Lawrence, *Accounts of Chemical Research*, 2015, **48**, 2866-2874.

53. J. Manuel Ortiz-Guerrero, M. Carmen Polanco, F. J. Murillo, S. Padmanabhan and M. Elias-Arnanz, *Proceedings of the National Academy of Sciences of the United States of America*, 2011, **108**, 7565-7570.

54. M. Jost, J. Fernandez-Zapata, M. C. Polanco, J. M. Ortiz-Guerrero, P. Y.-T. Chen, G. Kang, S. Padmanabhan, M. Elias-Arnanz and C. L. Drennan, *Nature*, 2015, **526**, 536-541.

Dalton Transactions Accepted Manuscript

55.   R. J. Kutta, S. J. O. Hardman, L. O. Johannissen, B. Bellina, H. L. Messiha, J. M. Ortiz-Guerrero, M. Elias-Arnanz, S. Padmanabhan, P. Barran, N. S. Scrutton and A. R. Jones, *Nature Communications*, 2015, **6**.

56.   R. J. Sension, A. G. Cole, A. D. Harris, C. C. Fox, N. W. Woodbury, S. Lin and E. N. G. Marsh, *Journal of the American Chemical Society*, 2004, **126**, 1598-1599.

57.   R. J. Sension, D. A. Harris, A. Stickrath, A. G. Cole, C. C. Fox and E. N. G. Marsh, *The Journal of Physical Chemistry B*, 2005, **109**, 18146-18152.

58.   H. J. Russell, A. R. Jones, S. Hay, G. M. Greetham, M. Towrie and N. S. Scrutton, *Angewandte Chemie-International Edition*, 2012, **51**, 9306-9310.

59.   W. D. Robertson, M. Wang and K. Warncke, *Journal of the American Chemical Society*, 2011, **133**, 6968-6977.

60.   A. R. Jones, S. J. O. Hardman, S. Hay and N. S. Scrutton, *Angewandte Chemie-International Edition*, 2011, **50**, 10843-10846.

61.   W. D. Robertson and K. Warncke, *Biochemistry*, 2009, **48**, 140-147.

62.   A. R. Jones, C. Levy, S. Hay and N. S. Scrutton, *Febs Journal*, 2013, **280**, 2997-3008.

63.   T. A. Shell and D. S. Lawrence, *Journal of the American Chemical Society*, 2011, **133**, 2148-2150.

64.   T. E. Wiley, W. R. Miller, N. A. Miller, R. J. Sension, P. Lodowski, M. Jaworska and P. M. Kozlowski, *The Journal of Physical Chemistry Letters*, 2016, **7**, 143-147.

65.   M. Jaworska, P. Lodowski, T. Andruniow and P. M. Kozlowski, *Journal of Physical Chemistry B*, 2007, **111**, 2419-2422.

66.   P. Lodowski, M. Jaworska, T. Andruniow, M. Kumar and P. M. Kozlowski, *Journal of Physical Chemistry B*, 2009, **113**, 6898-6909.

67.   P. Lodowski, M. Jaworska, K. Kornobis, T. Andruniow and P. M. Kozlowski, *Journal of Physical Chemistry B*, 2011, **115**, 13304-13319.

68.   M. Kumar and P. M. Kozlowski, *Chemical Physics Letters*, 2012, **543**, 133-136.

69.   H. Liu Hui, K. Kornobis, P. Lodowski, M. Jaworska and P. M. Kozlowski, *Frontiers in chemistry*, 2013, **1**.

70.   P. Lodowski, M. Jaworska, T. Andruniow, B. D. Garabato and P. M. Kozlowski, *Physical Chemistry Chemical Physics*, 2014, **16**, 18675-18679.

71.   P. Lodowski, M. Jaworska, T. Andruniow, B. D. Garabato and P. M. Kozlowski, *Journal of Physical Chemistry A*, 2014, **118**, 11718-11734.

72.   P. Lodowski, M. Jaworska, B. D. Garabato and P. M. Kozowski, *Journal of Physical Chemistry A*, 2015, **119**, 3913-3928.

73.   B. D. Garabato, N. Kumar, P. Lodowski, M. Jaworska and P. M. Kozlowski, *Physical Chemistry Chemical Physics*, 2015, DOI: 10.1039/C5CP06439B.

74.   T. Andruniow, P. Lodowski, B. D. Garabato, M. Jaworska and P. M. Kozlowski, *Journal of Chemical Physics*, 2015, Submitted 2015, Manuscript #C15.12.0206

75.   L. Randaccio, M. Furlan, S. Geremia, M. Šlouf, I. Srnova and D. Toffoli, *Inorganic Chemistry*, 2000, **39**, 3403-3413.

76.   L. Z. Ouyang, P. Rulis, W. Y. Ching, G. Nardin and L. Randaccio, *Inorganic Chemistry*, 2004, **43**, 1235-1241.

77.   L. Z. Ouyang, P. Rulis, W. Y. Ching, M. Slouf, G. Nardin and L. Randaccio, *Spectrochimica Acta Part a-Molecular and Biomolecular Spectroscopy*, 2005, **61**, 1647-1652.

78.   L. Randaccio, S. Geremia, G. Nardin and J. Wuerges, *Coordination Chemistry Reviews*, 2006, **250**, 1332-1350.

79.   J. Wuerges, L. Randaccio, N. Demitri and S. Geremia, *Trends in Inorganic Chemistry*, 2009, **11**, 1-19.

80.   J. Kuta, S. Patchkovskii, M. Z. Zgierski and P. M. Kozlowski, *Journal of Computational Chemistry*, 2006, **27**, 1429-1437.
81.   K. P. Jensen and U. Ryde, *Coordination Chemistry Reviews*, 2009, **253**, 769-778.
82.   K. Kornobis, N. Kumar, B. M. Wong, P. Lodowski, M. Jaworska, T. Andruniow, K. Ruud and P. M. Kozlowski, *Journal of Physical Chemistry A*, 2011, **115**, 1280-1292.
83.   K. Kornobis, N. Kumar, P. Lodowski, M. Jaworska, P. Piecuch, J. J. Lutz, B. M. Wong and P. M. Kozlowski, *Journal of Computational Chemistry*, 2013, **34**, 987-1004.
84.   K. Kornobis, K. Ruud and P. M. Kozlowski, *Journal of Physical Chemistry A*, 2013, **117**, 863-876.
85.   E. Runge and E. K. U. Gross, *Physical Review Letters*, 1984, **52**, 997-1000.
86.   M. E. Casida, in *Recent Developments and Application of Modern Density Functional Theory*, ed. J. M. Seminario, Elsevier, Amsterdam, 1996, pp. 391-439.
87.   E. J. Baerends, G. Ricciardi, A. Rosa and S. J. A. van Gisbergen, *Coordination Chemistry Reviews*, 2002, **230**, 5-27.
88.   A. Dreuw and M. Head-Gordon, *Chemical Reviews*, 2005, **105**, 4009-4037.
89.   A. Dreuw, *Chemphyschem*, 2006, **7**, 2259-2274.
90.   K. P. Jensen and U. Ryde, *Journal of Physical Chemistry A*, 2003, **107**, 7539-7545.
91.   P. M. Kozlowski, M. Kumar, P. Piecuch, W. Li, N. P. Bauman, J. A. Hansen, P. Lodowski and M. Jaworska, *Journal of Chemical Theory and Computation*, 2012, **8**, 1870-1894.
92.   U. Ryde, R. A. Mata and S. Grimme, *Dalton transactions*, 2011, **40**, 11176-11183.
93.   H. Hirao, *Journal of Physical Chemistry A*, 2011, **115**, 9308-9313.
94.   K. P. Kepp, *Journal of Physical Chemistry A*, 2014, **118**, 7104-7117.
95.   Z.-w. Qu, A. Hansen and S. Grimme, *Journal of Chemical Theory and Computation*, 2015, **11**, 1037-1045.
96.   T. A. Stich, A. J. Brooks, N. R. Buan and T. C. Brunold, *Journal of the American Chemical Society*, 2003, **125**, 5897-5914.
97.   J. Kuta, J. Wuerges, L. Randaccio and P. M. Kozlowski, *Journal of Physical Chemistry A*, 2009, **113**, 11604-11612.
98.   C. Rovira and P. M. Kozlowski, *Journal of Physical Chemistry B*, 2007, **111**, 3251-3257.
99.   T. Andruniow, M. Jaworska, P. Lodowski, M. Z. Zgierski, R. Dreos, L. Randaccio and P. M. Kozlowski, *Journal of Chemical Physics*, 2008, **129**.
100.   T. Andruniow, M. Jaworska, P. Lodowski, M. Z. Zgierski, R. Dreos, L. Randaccio and P. M. Kozlowski, *Journal of Chemical Physics*, 2009, **131**.
101.   A. R. Jones, J. R. Woodward and N. S. Scrutton, *Journal of the American Chemical Society*, 2009, **131**, 17246-17253.
102.   L. D. Landau, *Phys. Soviet Union*, 1932, **II**, 46–51.
103.   S. K. Lower and E.-S. M. A., *Chem Rev*, 1966, **66**, 199-241.
104.   C. M. Marian, *Wiley Interdisciplinary Reviews-Computational Molecular Science*, 2012, **2**, 187-203.
105.   J. M. Pratt, *Journal of the American Chemical Society*, 1964, 5154-5160.
106.   H. P. Hogenkamp, *Ann. N. Y. Acad. Sci.*, 1964, **112**, 552-564.
107.   H. P. Hogenkamp, *Biochemistry*, 1966, **5**, 417-422.
108.   K. Bernhauer, O. Mueller and F. Wagner, *Agnew. Chem. Int. Ed. Engl.*, 1964, **3**, 200-211.
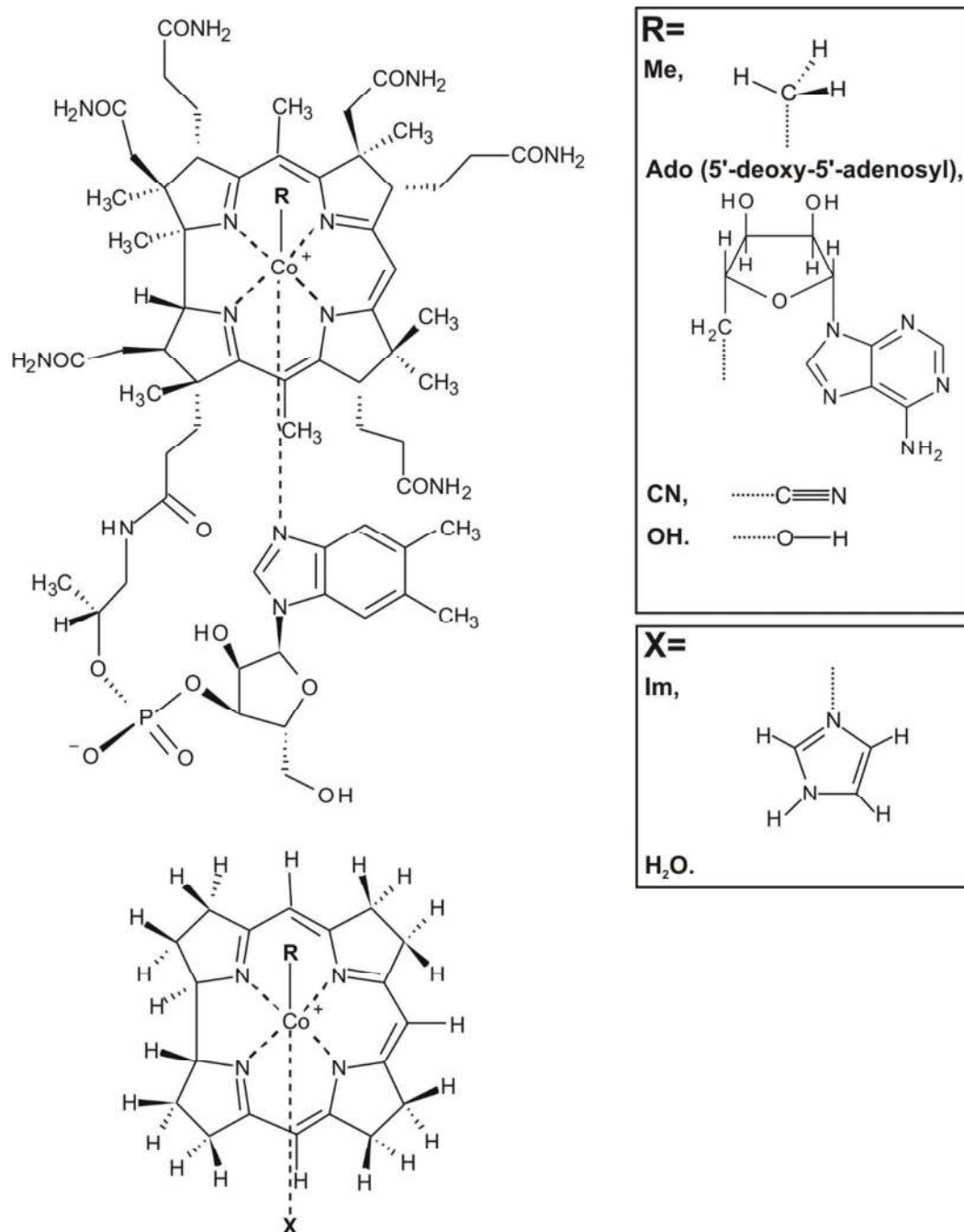
Figure 1. Molecular structure of cobalamins (upper). Truncated model used in DFT and TD-DFT calculations (lower).
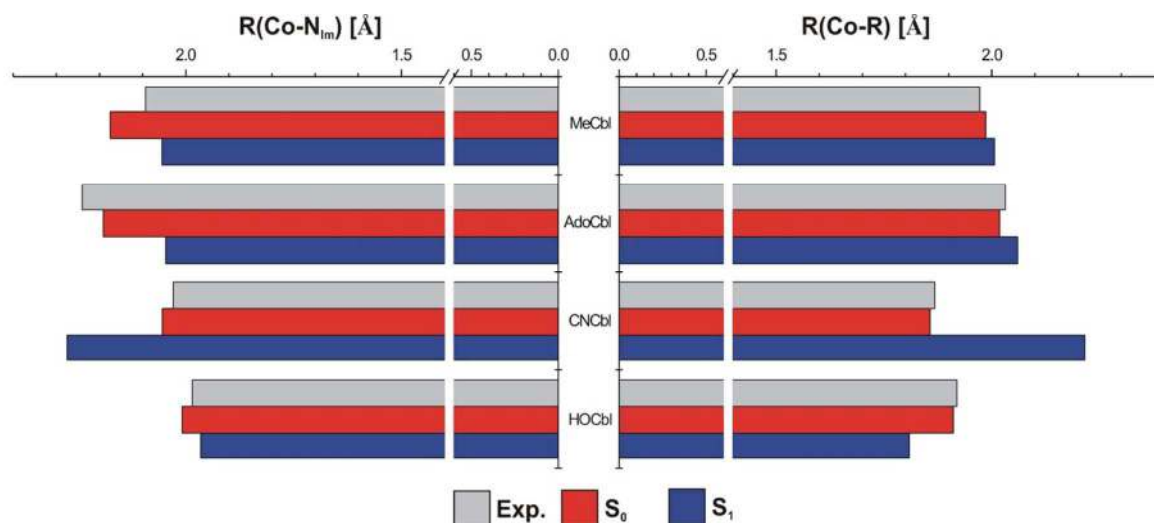
Figure 2. Experimental, and optimized axial bond lengths at the DFT/BP86 level, for S_0 and TD-DFT/BP86 for S_1 excited states of the cobalamins under consideration (MeCbl,[74] AdoCbl,[75] CNCbl,[77] HOCbl [76]). In all calculations the same basis sets, TZVPP for Co, C, N, and TZVP for H were used, employing the Conductor-like Screening Model (COSMO) solvent.
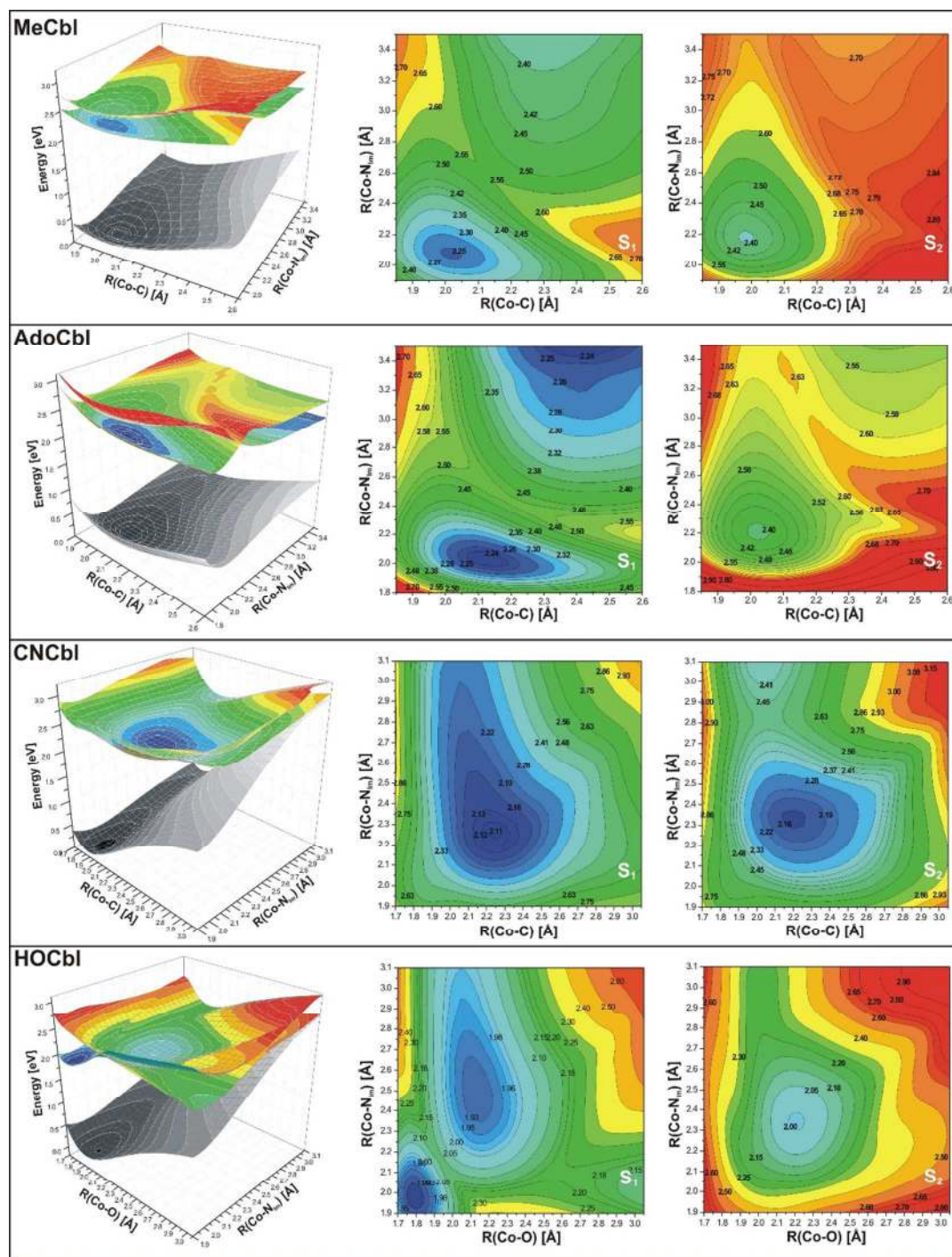
Dalton Transactions Accepted Manuscript

Figure 3. Potential energy surfaces for the singlet ground, and two lowest excited states of the cobalamins under consideration (MeCbl,[70,71] AdoCbl,[68] CNCbl,[66,69] HOCbl [63]) (left panel), along with vertical projections plotted as a function of axial bond lengths (right panel). In all calculations the BP86 functional was used, with TZVPP for Co, C, N, and TZVP for H basis sets, employing water as the COSMO solvent.
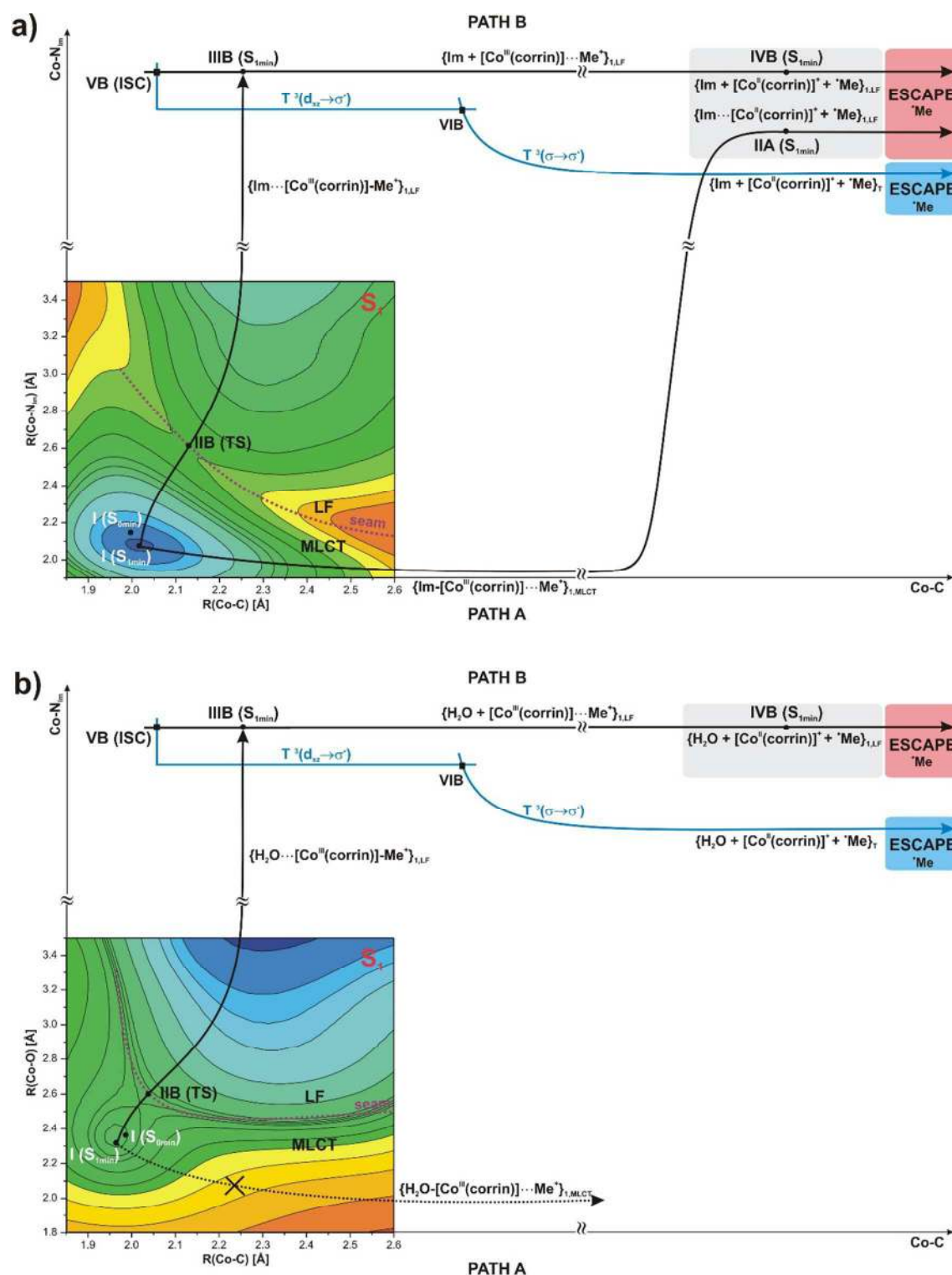
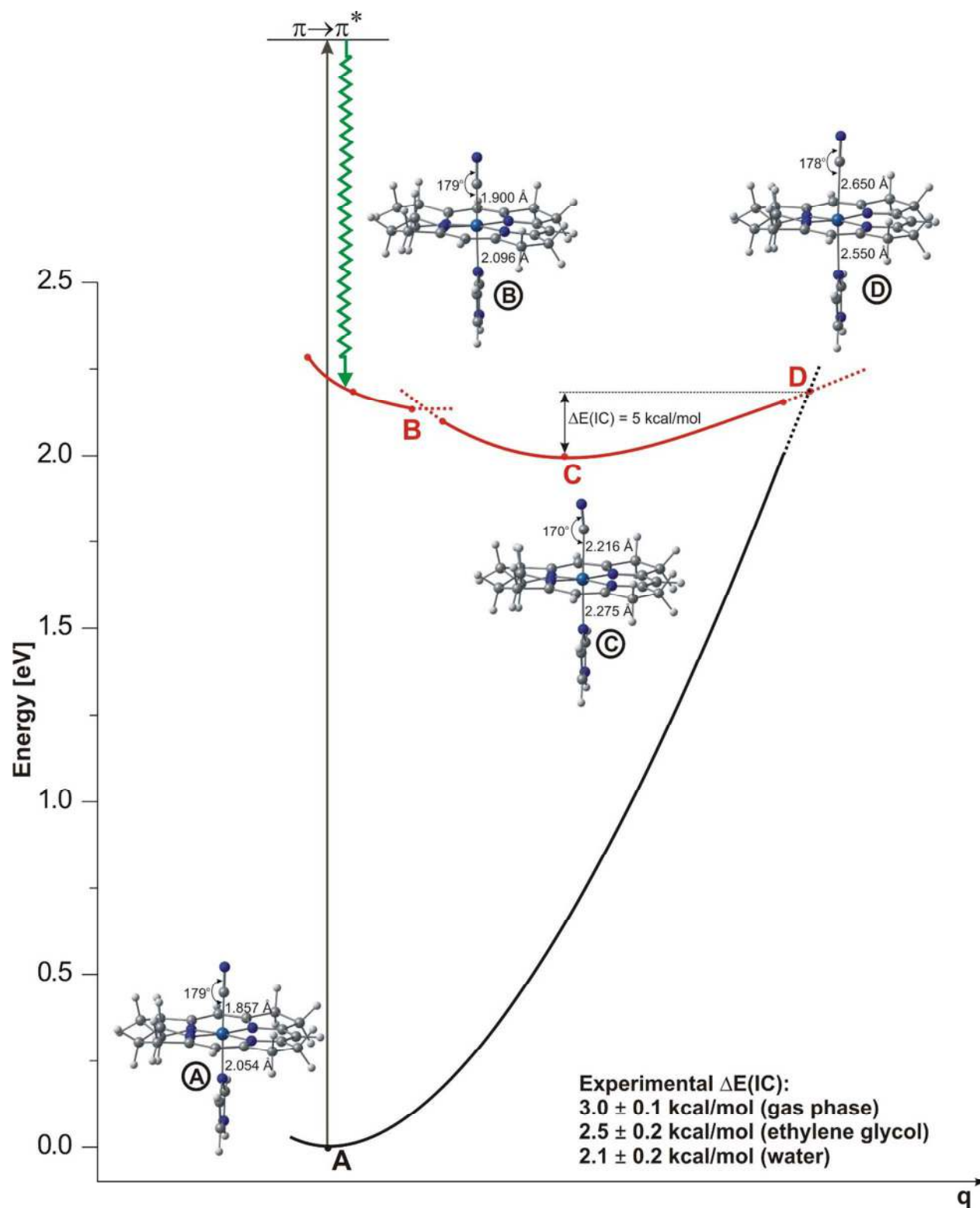**Figure 4.** Scheme of photoreaction on possible paths a) A and B for the base-on form of methylcobalamin,[70] b) B for the base-off form of methylcobalamin.[71] Path A is not active for the base-off form. In all calculations the BP86 functional was used, with TZVPP for Co, C, N, and TZVP for H basis sets, employing water as the COSMO solvent.

Figure 5. Schematic representation of the diagonal cut bisecting the S_1 PES of CNCbl. In all calculations the BP86 functional was used, with TZVPP for Co, C, N, and TZVP for H basis sets, employing water as the COSMO solvent.[69]
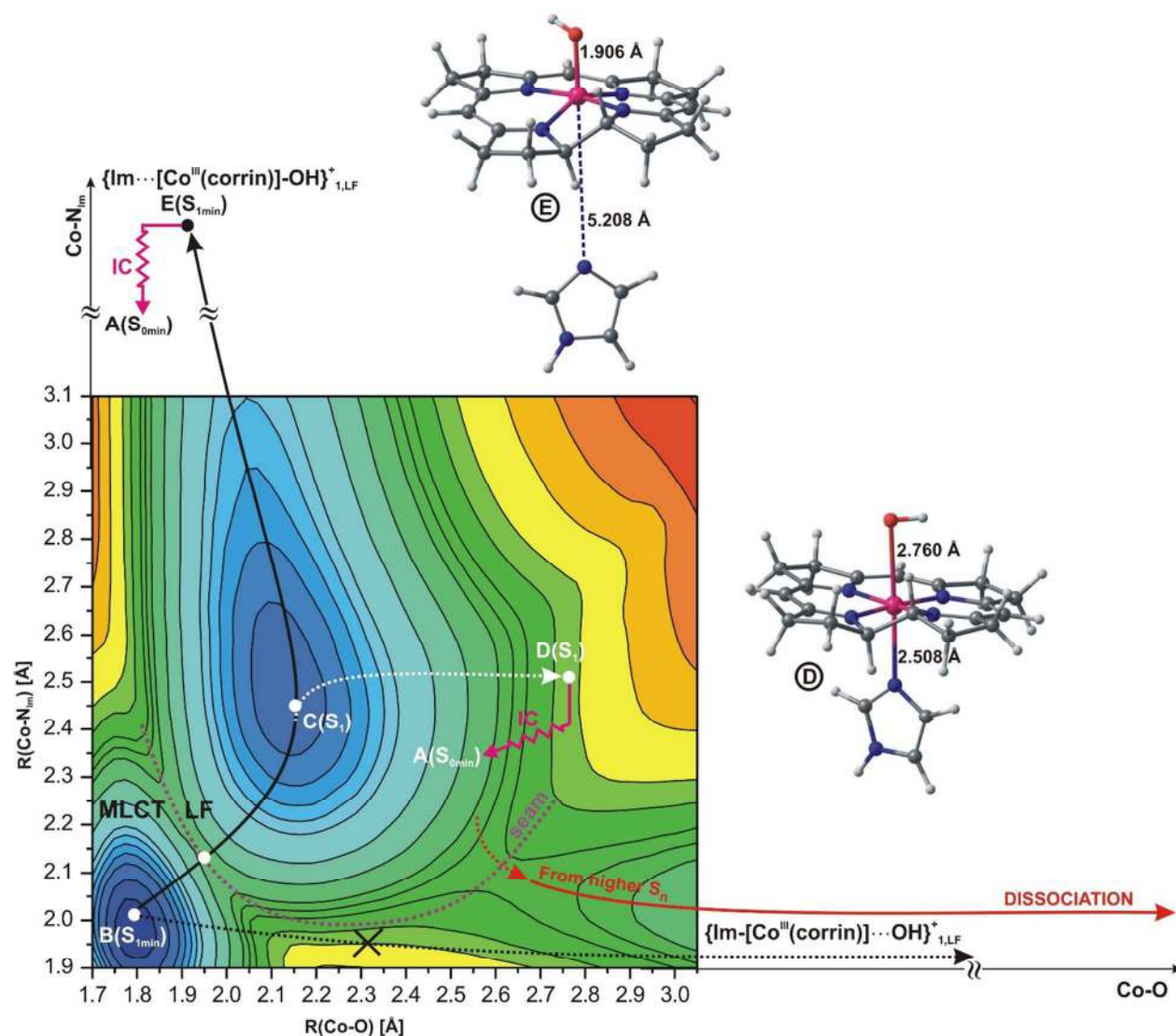
Figure 6. Potential energy surface of hydroxocobalamin shown with minimum energy paths leading to IC, and possible dissociation. In all calculations the BP86 functional was used, with TZVPP for Co, C, N, and TZVP for H basis sets, employing water as the COSMO solvent.[63]
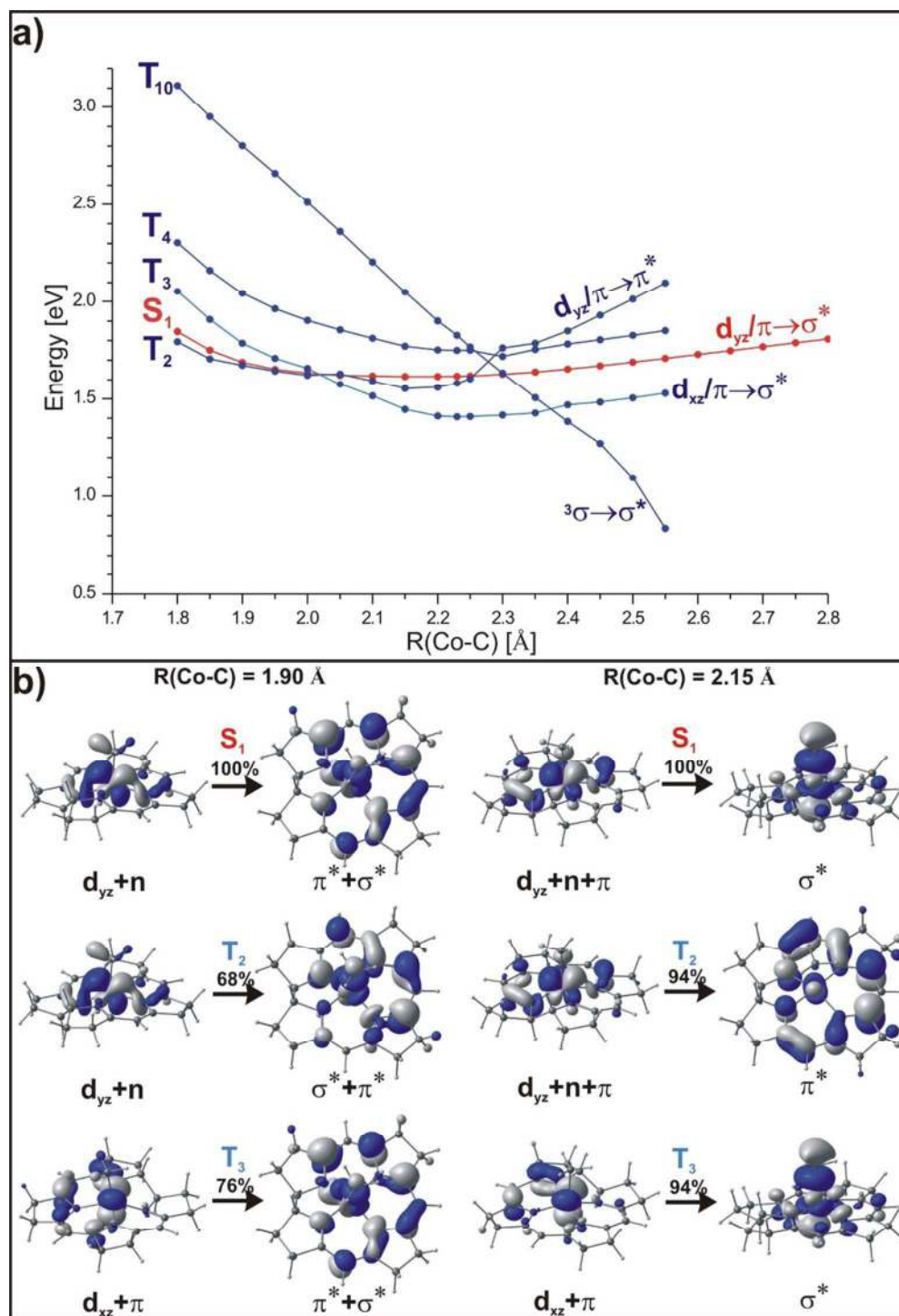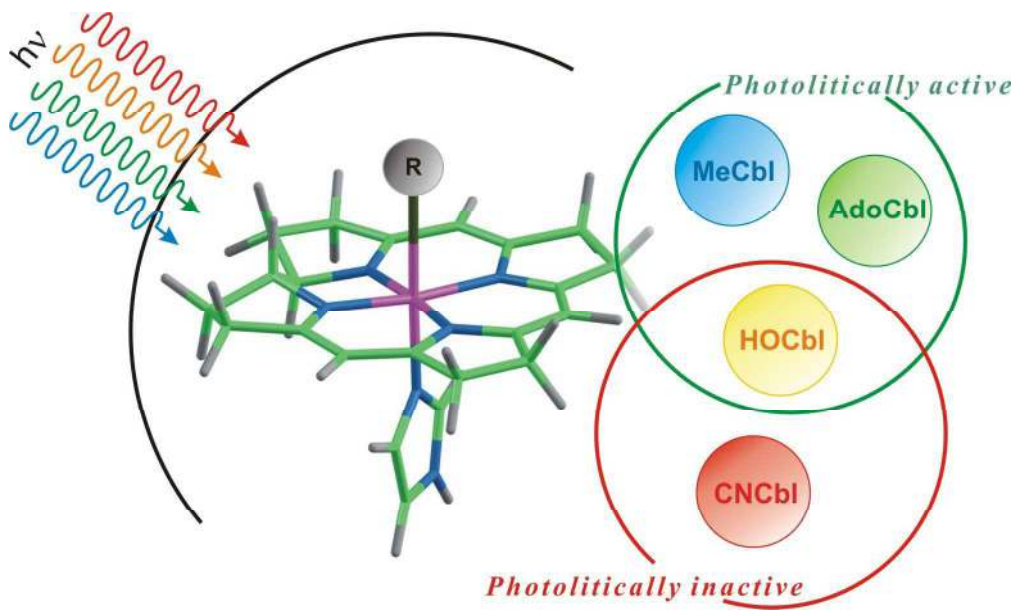
Dalton Transactions Accepted Manuscript

Figure 7 Potential energy curves of the ground (S_0) and selected lowest singlet (S_1), and triplet (T_1, T_2, T_3, T_4) excited states, as well as the repulsive $^3(\sigma \rightarrow \sigma*)$ state, for the $[Co^{III}(corrin)]-Me^+$ model complex along the Co−C coordinate of the optimized S_1 state.[71] (b) Molecular orbitals (MOs) describing the singlet and triplet excited state character for two different Co−C distances, R(Co-C)=1.90Å, and 2.15 Å corresponding to points before and after the MECP where intersystem crossing at each point may occur between S_1 and T_3.

178x106mm (300 x 300 DPI)